THE BAROCLINIC INSTABILITY OF THE TWO-DIMENSIONAL VARIABLE-DENSITY MIXING LAYER

Jean Reinaud and Laurent Joly
Department of Fluids Mechanics, E.N.S.I.C.A.
Toulouse, 31056, France

Patrick Chassaing
Institut de Mécanique des Fluides de Toulouse
Toulouse, 31400, France

ABSTRACT

The development of a small-scale, secondary roll-up in an incompressible, inviscid, variable-density, high Froude number, two-dimensional mixing layer is numerically investigated using the Transport Element Method. The numerical scheme consists in following a collection of elements carrying the local value of both the vorticity field and the density gradient. High resolution simulations of the temporal and spatial models of the shear layer are performed. They allow to capture the small-scale structures appearing over the primary Kelvin-Helmholtz instability where the baroclinic torque intensifies the vorticity field. Those results in contrast with the uniform density case, reveal the features of the variable-density transition to turbulence in variable-density shear flows.

INTRODUCTION

Within the context of variable-density shear flows, the generation-destruction of vorticity by the baroclinic torque may substantially alter the dynamics of the flow. Staquet (1995) has shown that the two-dimensionnal stratified mixing layer in a spanwise gravity field exhibits small-scale secondary eddies located at the saddle points between large-scale structures. In a compressible mixing layer, Lele (1989) indicated that the baroclinic torque may be invoqued together with the dilatation to explain the Mach number effect on the spreading rate. Our focus is on baroclinic effects beyond the Boussinesq approximation but uncorrelated to compressibility. This purely inertial influence of density variations is likely to occur in high Reynolds number mixing of fluids of different densities or in thermal mixing.

In the frame of the statistical approach, Chassaing et al. (1994) stressed the role of the correlations with density fluctuations in turbulent variable-density jets. Direct numerical simulations have been performed, see Chassaing et al. (1997) and Joly et al. (1997), that focus on the baroclinic forcing of a turbulent medium. The present contribution is a step toward the identification of a secondary baroclinic instability in the two-dimensional shear layer. Primary results on the temporally evolving periodic case, initiated in Reinaud and Joly (1998), are further investigated. Then a numerical simulation of a spatially evolving layer confirms the occurence of the baroclinic mode, a result in contrast with the simulations by Soteriou and Ghoniem (1995).

THE BAROCLINIC TORQUE

The baroclinic effect is the additionnal torque that is felt when an inhomogeneous mass field is submitted to a pressure gradient normal to the local density gradient. In the limit of inviscid two-dimensionnal incompressible flows, the baroclinic torque is the only source of vorticity variation along the particle path, as stated by the corresponding vorticity equations :

$$\mathrm{d}_t\,\omega = -\frac{1}{\rho^2}\boldsymbol{\nabla} P \times \boldsymbol{\nabla}\rho \qquad (1)$$

where $\mathrm{d}_t = \partial_t + \mathrm{u}\cdot\boldsymbol{\nabla}$ is the material derivative. In this simplified situation the pressure gradient is directly connected to the material acceleration $\mathrm{a} = \mathrm{d}\mathrm{u}/\mathrm{d}t$ such that the baroclinic torque b reads :

$$\mathrm{b} = \mathrm{a} \times \boldsymbol{\nabla}(\ln\rho) \qquad (2)$$

Hence the interpretation of the baroclinic torque as being of inertial nature. The Lagrangian approach, han-

dling directly the material acceleration, is particularly suited for the simulation of such a problem as it avoids the resolution of a Poisson equation for the pressure. The free shear layer is also a case where vorticity is concentrated on a bounded domain and this indicates an expected computationnal efficiency of the method.

NUNERICAL PROCEDURES

Following Ghoniem et al.(1988), the so-called "Blob vortex method" originated by Chorin (1973) can be generalized to perform simulations of variable-density flows. The numerical procedure aims at tracking a collection of n Lagrangian elements transporting both the local value of the vorticity and the density gradient on a radially symmetric core, characterized by the "cut-off" function f_δ. The basic equations are the Lagrangian vortex element displacement :

$$\mathrm{d}_t\, \mathrm{x}_i = \mathrm{u}(\mathrm{x}_i, t) \tag{3}$$

$$\mathrm{u}(\mathrm{x}, t) = \iint K_\delta(\mathrm{x} - \mathrm{x}')\, \omega(\mathrm{x}', t)\, \mathrm{dx}' \tag{4}$$

where $K_\delta = K * f_\delta$ is the convolution product between the kernel of the Biot-Savart integral K and the "cut-off" -or desingularisation- function f_δ, and the vorticity transport equation (1). They are evolved in time simultaneously using Runge-Kutta schemes. Both acceleration and density gradient fields have to be updated at each calculation step. The acceleration of the transport elements is obtained by a second-order backward finite difference scheme. The density gradient is deduced from the local stretching of an isopicnic line according to the following equation :

$$\frac{|\nabla\rho|}{|\mathrm{d}\ell|} = cst \qquad \text{and} \qquad \nabla\rho \cdot \mathrm{d}\ell = 0 \tag{5}$$

In the discrete description of the flow map, the local stretching around an element is obtained from the knowledge of the location of the neighbouring elements of the same isopicnic line. Then, by considering that

$$\Delta\rho = \nabla \cdot \nabla\rho \tag{6}$$

the density field can be obtained using the reconstruction formula (Anderson, 1980) :

$$\rho(\mathrm{x}, t) = \iint L_\delta(\mathrm{x} - \mathrm{x}') \cdot \nabla\rho(\mathrm{x}', t)\, \mathrm{dx}' + \rho_p \tag{7}$$

where ρ_p is a constant depending on the boundary conditions and $L_\delta = L * f_\delta$ is the desingularised gradient of the two-dimensional Green function with

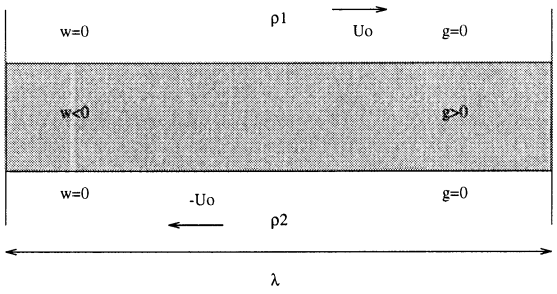

Figure 1: The temporal model (g stands for $\nabla\rho$)

$$L(\mathrm{x}) = \frac{1}{2\pi r^2}(x, y) \tag{8}$$

A Lagrangian spatial refinement strategy, which inserts or removes elements along isopicnic lines, is adopted which ensures the required overlap between neighbouring blob elements (Leonard, 1980).

THE TEMPORAL MIXING LAYER

In those simulations, the temporal integration of the transport equations (1 and 3) is performed using a fourth-order Runge-Kutta scheme. The kernel of the Biot-Savart law is desingularised using gaussian functions and leads, in the present case, to a fourth-order spatial accuracy for the velocity field (Beale and Majda,1985).

The initial condition is a gaussian vorticity layer tilted by an harmonic spatial perturbation on which a density gradient layer of the same thickness is superimposed. This model is in good agreement with the experimental mean velocity and density profiles near the trailing edge of a plane splitter plate, see Brown and Roshko, 1974. Periodicity is assumed in the streamwise direction and is set to the most unstable wavelenght of the constant-density case $\lambda = 13.2\sigma$ where σ is the standard deviation of the initial vorticity profile (Ghoniem et al., 1988). The geometry is described on figure 1.

The periodic boundary condition is treated analytically by evaluating the velocity field induced by any vortex in the computation domain and its infinite row of images in the other periods (Ghoniem et al., 1988).

The circulation over a period is demonstrated to remain constant and gives a fair validation of the simulations ($\Gamma = -\lambda\Delta U$).

Moreover, the temporal model allows to perform high resolution simulations of the initial stage of the Kelvin-Helmholtz roll-up because of the restriction of the computational domain to a single main structure.

The problem is normalized by the velocity scale $\Delta U/2$, the density ρ_2 of the bottom flow and the length scale σ. The temporal evolution of the reduced circulation is presented in figure 2 in the case where the initial layer is mapped with 73 isopicnic lines and each lines is

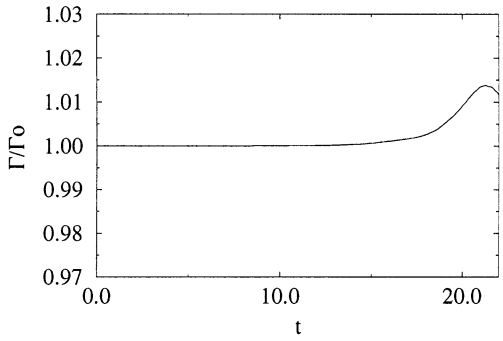

Figure 2: Temporal evolution of the reduced circulation over a period of the temporal model for ρ_1/ρ_2=3.0. The initial layer is mapped with 73 isopicnic lines and each line is mapped with 264 elements.

discretized with 264 elements. Then, the relative error on the circulation is kept under 1.5% till $t = 22.0$.

As noted by Soteriou and Ghoniem (1995), during the roll-up of the primary Kelvin-Helmholtz instability, an element in the braid experiences an accelerelation that advects it toward the vortical core. The local density gradient sets the sign of the baroclinic torque contribution to the vorticity field such that vorticity is created in the light-side braid of the main structure and destroyed inside the heavy-side braid. It should be noted that vorticity may even exhibit positive values. Those facts are relevent of both the temporal and the spatial models of the shear layer. This results in a substantial change and dissymmetry of the vorticity pattern as compared to the constant-density one.

Moreover the present paper stresses that the combination of the natural straining field and the intensification of the vorticity in the light-side braid yields a highly unstable sublayer that breaks into a row of growing secondary structures. This sublayer is allowed to evolve in time and space within the periodic time-evolving box and is identified as a baroclinic secondary instability. The figure 3 illustrates the evidence of the secondary mode against the equivalent constant density vorticity field. The invariance of the sequence of small-scale eddies against spatial and temporal resolution has been previously established (Reinaud and Joly, 1998). The figures 4 that represent instantaneous spectra of the enstrophy repartition over a period at $t = 20.0$ and $t = 21.0$, also reveal the specificity of the variable-density case as this repartition is radically different for the two cases. In the variable-density case, it is shown that enstrophy develops high wave number modes.

Additionnal simulations, performed on a two-period box with a pairing mode also exited, indicate that the baroclinic break-up of the light-side braid may occur well before the pairing has completed (Reinaud and Joly, 1998). This motivates the investigation of the more realistic, spatially developping shear layer.

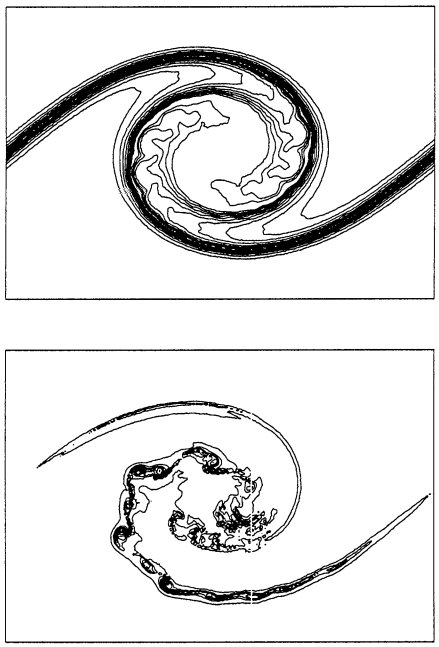

Figure 3: Iso-vorticity contours at $t = 20.0$ for temporal mixing layers. Case I : uniform density, Case II : variable density ($\rho_1/\rho_2 = 3.0$)

THE SPATIAL MIXING LAYER

The temporal integration of equation (1 and 3) is performed using a second order Runge-Kutta scheme. The spatial accuracy is also reduced to enhance the robustness of calculation in the intense gradient region. The vorticity profile in the inlet section is gaussian and the layer is confined between two free-slip walls. The computational domain is a troncated vorticity layer with length X_{max}. The walls are taken into account by a Schwartz-Christoffel conformal mapping of the physical space into the upper half plane. As proposed first by Ghoniem and Ng (1987), an appropriate system of images ensures a zero normal velocity at the walls. The upstream uniform flows are represented by point volume sources placed (in the physical space) at $(-\infty, 0^-)$ and $(-\infty, 0^+)$. The elements are introduced in the computational domain according to the Kutta condition. The downstream condition consists in deleting the elements as they cross the exit section of the computational domain. This assumption, though generating errors near the exit section, is commonly used in vortex methods.

The geometry of the configuration is given in figure 5. The layer is forced with the most unstable mode of the uniform density case and its first surbharmonic. The problem is normalized by the velocity scale U_1, the density ρ_2 of the top stream and the length scale H, height of the channel. The standard deviation σ of

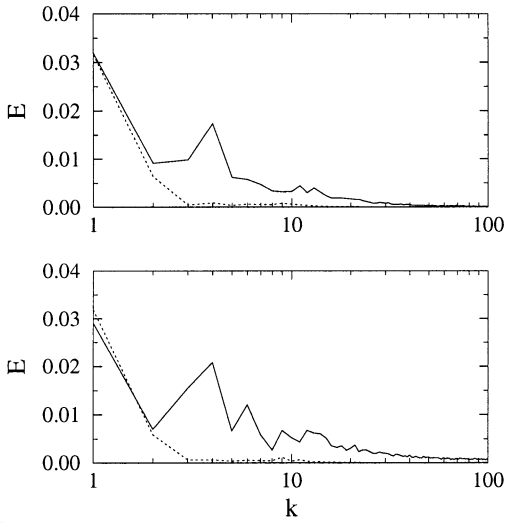

Figure 4: Enstrophy spectra over a period of the temporal model for ρ_1/ρ_2=3.0 (solid line) and ρ_1/ρ_2=1.0 (dashed line) at $t = 20.0$ and $t = 21.0$

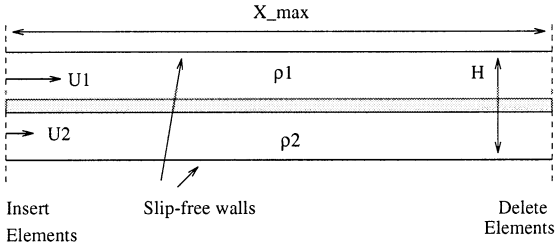

Figure 5: Geometry of the spatial model

both the vorticity and the density gradient profiles at the inlet section is scaled so that $\sigma = H/(2\lambda)$ where λ is the most instable wavelenght of the uniform density case. This choice allows the pairing mode to appear without being constrained by the presence of the walls (Ghoniem and Ng, 1986).

The figures 6-10 show the location of the elements over the vortical domain for 5 different computational settings. When comparing the figures 6 and 7, the influence of the exit condition can be seen to be weak. As quoted by Soteriou and Ghoniem (1995), the results are affected on an upward distance corresponding to the channel height H. The rather poorly resolved simulations are showing a very good agreement with the results obtained by the authors.

As in the temporally evolving layer, an increase in the spatial resolution between the cases reported in figures 7, 8 and 9, reveals secondary roll-ups while the main structures location is unchanged. Those roll-ups are the signature of an additional instability mechanism over the constant density case reported for reference on figure 10.

The vorticity field (not illustrated here) reveals a much more intricated pattern before the pairing. The pairing phenomena itself is no more a pairing between two main structures but rather a pairing of two dipoles.

Though the fine description of small scale structures does not change the layer spreading rate, it is necessary to the description of the transition to turbulence in the variable density shear layer.

Conclusion

Highly resolved simulations of the temporally growing variable-density inviscid mixing layer reveal the presence of a secondary baroclinic instability. The spatio-temporal development of this secondary mode could be viewed as a smaller scale Kelvin-Helmholtz mode due to the stretching and baroclinic intensification of the vorticity light-side braid. The occurence of this secondary mode is demonstrated in the case of the spatially developping layer. It is concluded that the baroclinic forcing of a variable-density mixing layer ends in a transition towards turbulence radically different from the constant density one.

REFERENCES

Chassaing P., Harran G. and Joly L., 1994, "Density fluctuation correlations in free turbulent binary mixing" J. Fluid Mech., Vol. 279, pp. 239-278

Chassaing P., Castaldi S., Harran G. and Joly L., 1997, "Variable density mixing in kinematically homogeneous turbulence" 11th Conf. on Turb. Shear Flows.

Chorin A.J., 1973 "Numerical study of a slightly viscous flow", J. Fluid Mech., Vol 57 pp. 785.

Ghoniem A.F., Heidarinejad G., and Krishnan A., 1988, "On mixing, Baroclinicity and the Effect of Strain in a Chemically-Reacting Shear Layer" AIAA paper 88-0729.

Ghoniem A.F., Ng K.K., 1987, "Numerical study of the dynamics of a forced shear layer", Phys. Fluids 30(3), pp 706-721.

Joly L., Chassaing P. and Castaldi S., 1997, "Direct simulation of a variable density incompressible homogeneous turbulence" First AFOSR Int. Conf. on DNS-LES.

Lele S., 1989, CTR Report N89-22827, 1989.

Leonard A., 1980, "Vortex methods for flow simulation" J. Comp. Phys., Vol. 37, pp 289-335.

Reinaud J., Joly L. 1998, "Numerical simulation of a forced, variable-density, temporal mixing layer by Vortex Methods" 3rd Int. Workshop on Vortex Flows.

Soteriou M.C. and Ghoniem A.F., 1995, "Effects of the free-stream density ratio on free and forced spatially developing shear layers" Phys. Fluids A, 7(8), pp 2036-2051.

Staquet C.,1995, " Two-dimensional secondary instabilities in a stratified shear layer", J. Fluid Mech.,Vol. 296 pp 73-126.

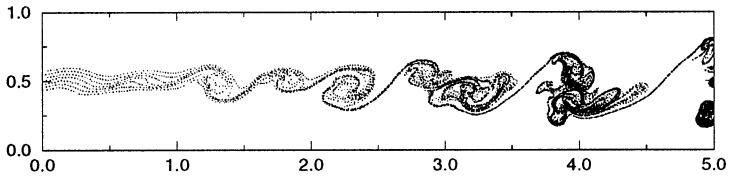

Figure 6. Location of the elements a $t = 8.0$ for a variable-density spatially developping shear layer with $U_2/U_1 = 0.5$ and $\rho_2/\rho_1 = 0.33$, $X_{max} = 5$, $h = 0.0234$ (initial spatial step)

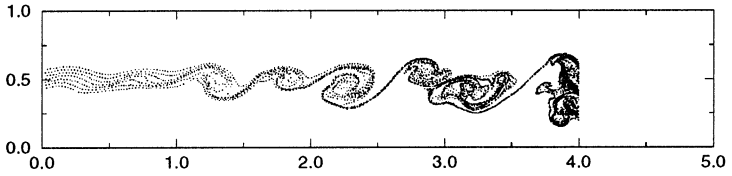

Figure 7. Location of the elements a $t = 8.0$ for a variable-density spatially developping shear layer with $U_2/U_1 = 0.5$ and $\rho_2/\rho_1 = 0.33$, $X_{max} = 4$, $h = 0.0234$ (initial spatial step)

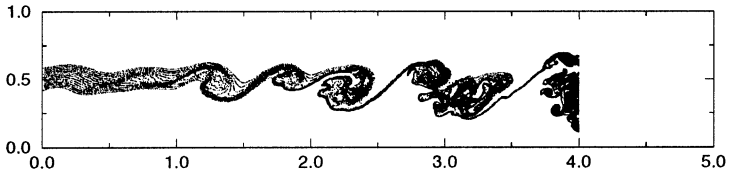

Figure 8. Location of the elements a $t = 8.0$ for a variable-density spatially developping shear layer with $U_2/U_1 = 0.5$ and $\rho_2/\rho_1 = 0.33$, $X_{max} = 4$, $h = 0.0117$ (initial spatial step)

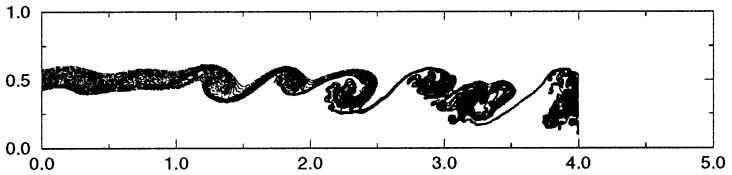

Figure 9. Location of the elements a $t = 8.0$ for a variable-density spatially developping shear layer with $U_2/U_1 = 0.5$ and $\rho_2/\rho_1 = 0.33$, $X_{max} = 4$, $h = 0.0078$ (initial spatial step)

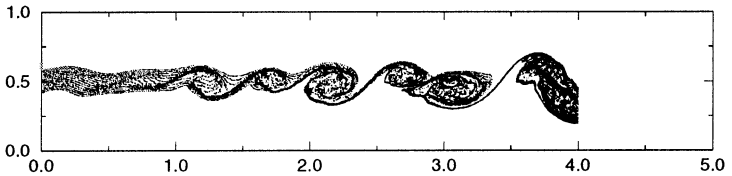

Figure 10. Location of the elements a $t = 8.0$ for a uniform-density spatially developping shear layer with $U_2/U_1 = 0.5$, $X_{max} = 4$, $h = 0.0117$ (initial spatial step)